L. Gagnon, G. Doré, M.J. Richard
An Overview of Various New Road Profile Quality Evaluation Criteria: Part 1
International Journal of Pavement Engineering, Vol. 16, N. 3, 2015, p. 224-238
doi:10.1080/10298436.2014.942814

This article is the final submission, post-review, version of the following article:

Gagnon, L., Doré, G., and Richard, M.J., « An overview of various new road profile quality evaluation criteria : part 1 », Int. J. of Pavement Engineering, 16(3):224-238, 2015,
doi: 10.1080/10298436.2014.942814

International Journal of Pavement Engineering
Vol. 00, No. 00, Month 2013, 1–24

RESEARCH ARTICLE

An overview of various new road profile quality evaluation criteria : part 1

Louis Gagnon,[a*] Guy Doré,[b]

and Marc J. Richard[a]

[a]*Department of Mechanical Engineering, Laval University, Québec, QC, Canada*;
[b]*Department of Civil Engineering, Laval University, Québec, QC, Canada*

(*Submitted for review*)

A multibody tractor-trailer model specialised in measuring the impact of road surface quality on the efficiency of transport was developed. It was calibrated and validated using a coastdown tests experimental campaign. The model was then used within an extensive profile study that linked specific profiles to their impact on energy consumption, vehicle wear, driver and passenger health, and safety. Two hundred and seventy 1 km long profiles were tested with the multibody vehicle travelling at 100 km/h. It allowed to identify trends in the relationships between various profile rating criteria and the impacts aforementioned. The criteria consist of 19 indices observed on a quarter car model operating on longitudinal road profiles. They yield accurate predictions of profile impacts. For the operating conditions considered, the long wavelengths have a strong effect on health, medium wavelengths on safety, and short to medium wavelengths on energy consumption.

Keywords: road roughness; IRI; quarter car; fuel efficiency; safety; health; multibody dynamics)

1. Introduction

The smoothness of the road surface has an undeniable influence on vehicle efficiency and poor roads incur a cost to vehicle operators. A thorough literature review lead Gagnon *et al.* (2006) to conclude that vehicle efficiency decreases when the road deteriorates. The negative consequences of a poor road surface quality can be broken down in different categories: fuel consumption (Velinsky and White 1980, Wambold 1985, Delanne 1994, Gyenes and Mitchell 1994, McLean and Foley 1998, Jackson 2004, Miege and Popov

*Corresponding author. Email: louis.gagnon.10@ulaval.ca

ISSN: 1029-8436 print/ISSN 1477-268X online

DOI: 10.1080/1029843YYxxxxxxxx
http://www.informaworld.com

2005, Fraggstedt 2006, Rhyne and Cron 2007, Jackson *et al.* 2011); driver and passenger wellness (Bouazara 1997, Fichera *et al.* 2007); and, safety (Sattaripour 1977, Bester 2003, Romão *et al.* 2003, Vassev 2005, Richard *et al.* 2009). The importance of those three impact categories has been outlined by the World Health Organization in various reports. For example, road traffic incidents are the eighth leading cause of mortality today (WHO 2013), gas emissions from vehicles give rise to pulmonary diseases which are also amongst the leading causes of death (WHO 2011), and low back pain is the major cause of morbidity worldwide (WHO 2002) and, coincidently, is widespread amongst heavy equipment operators.

Bearing that in mind, agencies responsible for the construction and maintenance of roads usually monitor the longitudinal profiles of their roads by taking profilometer readings. Although such readings are now standard procedure in developed countries, they usually only serve to compute the International Roughness Index (IRI). This index is widely used and is a calculation of the accumulated suspension movement of the Reference Quarter Car Simulation travelling at 80 km/h on the given profile. Typically, a road is considered to be in a splendid state when the IRI is between 1.0 and 1.5 m/km and in a horrible state when the IRI is above 5 m/km. For example, Pehlivanidis and St-Laurent (2001) report that, in 1999, the national roads of Quebec had an average IRI of 2.1 m/km while the collector roads had an average IRI of 3.1 m/km.

Hence, a semitrailer truck multibody model has been developed and validated in order to establish a precise link between a profile and its consequences. Fifty-four real 1 km long road profiles provided by Québec's *ministère des Transports* (MTQ) were analysed. They were taken from the up to date road database of the MTQ and selected in order to include from the smoothest to the worst road profiles. Each of these was used to generate 4 filtered profiles isolating the short, medium, long, and IRI wavelengths, thus yielding a total of 270 profiles. These filtered profiles derived from real ones are not likely to occur in real life but can trigger responses useful for research purposes. The truck model was driven in a straight line on each profile at a constant velocity of 100 km/h. This article presents the impact-index relations obtained and the trends identified after running the model on these 270 road profiles. It is the first of a two part article where the second part will cover the road impact on vehicle wear, a profile wavelength analysis method, and the particulars of the multibody model.

2. Methodology

This section summarises the approach taken to model the vehicle, run it on a profile, evaluate the impact from the road surface quality, and characterise the different profiles.

2.1. *Multibody model*

The multibody approach is the preferred choice of many authors when it comes to evaluating the aspects of energy consumption (Velinsky and White 1980, Lu 1985, Fichera *et al.* 2007, Stenvall 2010, Hammarström *et al.* 2012), occupant wellness (Bouazara 1991, 1997, Rakheja *et al.* 2001), and safety (Kollman 2007, Imine 2007). It was chosen to implement the model into the free and open-source software MBDyn (Masarati 2012, Masarati *et al.* 2014).

2.1.1. Tractor semitrailer

The semitrailer truck is implemented as a multibody model. It has 331 degrees of freedom (DoF) including the tyres. The chosen tractor is a conventional cab Freightliner Cascadia® and it tows a 16.2 m long three axle Manac® semitrailer. The total vehicle weight is 43 t. Apart from the wheels, the model has 13 rigid bodies having each 6 DoF : one for each axle; one for the chassis frame and the components which are rigidly attached to it, such as the batteries and gas tanks; one for the engine; one for the cabin; one for the driver and one for the passenger; one for the radiator; and, one for the semitrailer frame. The tractor and trailer are tied together by a spherical joint. The radiator is attached to the chassis by 2 uncoupled translational tridimensional viscoelastic elements. It is also constrained to prevent rotation about the tractor lateral axis by a cardano rotation joint, which is equivalent to two revolute joints placed orthogonal to each other. A side-view of the multibody truck model is shown in Figure 1

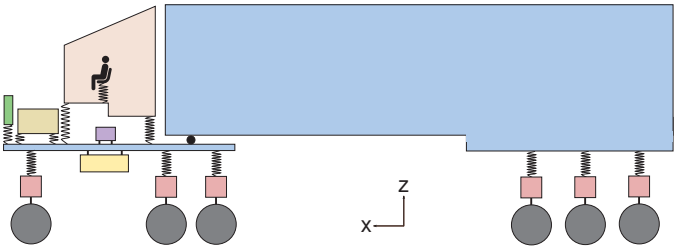

Figure 1. Sideview of the tridimensional truck model.

A steering algorithm similar to the moment-by-moment feedback models of Blundell and Harty (2004) is implemented. Its goal is to follow a straight line. The algorithm computes an error function which then gives a desired steering angle according to user set aggressivity factor and visibility distance parameters. This angle is then applied to the front wheels by an orientation constraint on their vertical axis.

Aerodynamic drag is accounted for by forces acting on the cabin and on the semitrailer in their longitudinal directions. It uses a calibrated truck drag coefficient to compute the drag force of which 55% acts on the cabin and 45% on the semitrailer, as derived from the data provided by Drollinger (1987).

Parasitic losses, which are the losses incurred by the wheel hub bearings, are applied as constant forces in the longitudinal direction of each axle.

Losses in the differential and in the transmission are used for the coastdown validation runs. They are applied as forces in the longitudinal direction of the two drive axles and they are calculated using a method given by Hammarström *et al.* (2012).

The complete tractor trailer model was calibrated and validated from the data obtained during an experimental campaign of coastdown tests where each run was repeated 5 times. Two sections of 518 m and 714 m lengths taken on an 80 km/h service road were tested in both directions thus resulting in 4 test segments. The segment's IRI varied between 5.9 m/km and 8.2 m/km and the individual track IRI varied between 5.1 m/km and 9.8 m/km, these are degenerate surface conditions. Such a high level of deterioration was chosen to ensure that the model is validated against road profiles that have a strong influence on the response of the vehicle. For the campaign, the procedure recommended by the J2263 norm (SAE 2008) was closely followed. Fourteen truck parameters were optimised to reproduce the experimental wheel-by-wheel weight distribution. Then, the calibration was carried on by adjusting the 40 acceleration curves and the 4 kinetic

energy loss calculations to the experimental data by adjusting another 16 model parameters consisting of the horizontal position of the semitrailer's center of mass and the static deflection of each suspension.

2.1.2. Multibody tyres

It was chosen to implement a rigid ring tyre model as a modification of the model of Gualdi *et al.* (2008) which was available in MBDyn. The implemented model is based on the *Short Wavelength Intermediate Frequency Tire* (SWIFT) model presented by Pacejka (2006) and it filters the road input using the method of Schmeitz (2004). The tyre model takes the three-dimensional forces and moments coming from the wheel of the truck model as one input (Gagnon *et al.* 2012). The other input to the tyre model is the road profile height. Its equations are implicitly integrated at each time step and the rotation parameters are handled by the updated-updated approach defined by Masarati (2000).

A simplified physical interpretation of the model is shown in Figure 2. It has three rigid elements. The inner element is referred to as the Wheel and comprises the wheel and any rotating mass attached to it, including a portion of the tyre sidewall, and is connected to the vehicle as a wheel hub assembly and allowed to roll. The outer element is referred to as the Ring and represents part of the sidewall, the belt, and the tread of the tyre and its purpose is to simulate the inertia of a rotating tyre. The external rigid element is a point mass referred to as the Patch and represents the translational inertia of the portion of the tread which exchanges friction and constraining forces with the ground. There are three independent translational viscoelastic elements that link the Wheel to the Ring and three that link the Ring to the Patch. There are also three independent torsional viscoelastic elements that link the Wheel to the Ring. The viscoelastic elements are implemented as noted by Masarati and Morandini (2010). The Patch is not subjected to gravity. Its height is dictated by its longitudinal position on the road and its vertical velocity is determined from its longitudinal velocity and the slope of the road profile. Slip forces obtained by the empirical formulae published by Pacejka (2006) are applied on the Patch.

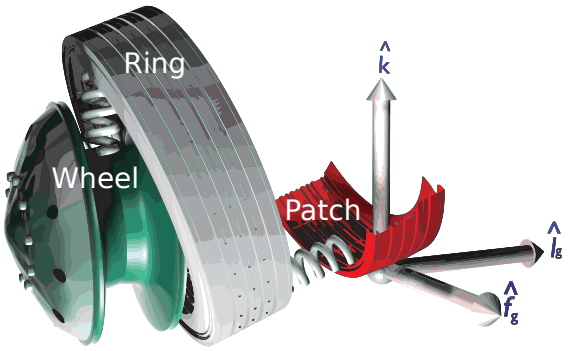

Figure 2. From left to right: Wheel, Ring, and Patch elements.

The calculated response of the tyre is precise for perturbation frequencies up to 100 Hz and for road protuberances up to 10 cm in height. It takes 45 tyre parameters and 20 algorithm parameters. The numerical integration is done implicitly except for the road profile data which uses data at the previous time step. The model was calibrated and validated by comparison to finite element analysis results provided by Michelin® for XZA-3 tyres assembled on a wheel attached to an axle and travelling over rectangular cleats. Above 20 km/h, the coefficient of determination R^2 was greater than 0.8 for all

vertical cleat force responses. As for the longitudinal forces, only one curve had a R^2 below 0.5.

2.2. *Profile evaluation procedure*

A profile evaluation study was conducted by using the developed truck model and running it at 100 km/h in a straight line on longitudinal road profiles. More than 200 one kilometre long profiles measured at 25 mm intervals were analysed. They represented paved roads of smoothness ranging from excellent to mediocre were analysed. In order to assess the full impact of the profile and nothing else, steps were taken to ensure that the vehicle was in equilibrium before entering and after leaving a profile. For the profile study, the truck velocity was controlled by an explicit cruise control algorithm which applies the same torque to each of the 8 drive wheels. The torque applied is function of the difference between targeted and actual vehicle velocities. It produces a maximum power of 274 kW which accounts for a 10% loss in the transmission.

2.2.1. Impact assessment

The three aforementioned impact categories are evaluated by examining the results of the multibody model runs. First, the quantity of energy q_{tot} that a particular profile dissipates is calculated from the following equation,

$$q_{\text{tot}} = \sum_{i=1}^{8} \left(\int_{x_{\text{in}}}^{x_{\text{out}}} \omega_i \tau_i dt \right) + \Delta E_{\text{k}} m_{\text{ck}} + \Delta E_{\text{p}} m_{\text{cp}} \tag{1}$$

where ω_i and τ_i are the angular velocity and torque applied to wheel i. The integral is taken on the profile section considered and m_{ck} and m_{cp} are the masses of the truck used for the kinetic and potential energy calculations, respectively. The variable ΔE_{p} is the quantity of potential energy per kilogramme that was lost on the profile and is calculated by the following equation,

$$\Delta E_{\text{p}} = (z_{\text{fra,in}} - z_{\text{fra,out}})\, \text{g} \tag{2}$$

where $z_{\text{fra,in}}$ and $z_{\text{fra,out}}$ are the respective vertical elevations of the truck frame at the start and at the end of the section considered and g is standard gravity. The lost kinetic energy per kilogramme ΔE_{k} is calculated from the following equation,

$$\Delta E_{\text{k}} = \frac{\dot{x}_{\text{fra,in}}^2 - \dot{x}_{\text{fra,out}}^2}{2} \tag{3}$$

where $\dot{x}_{\text{fra,in}}$ and $\dot{x}_{\text{fra,out}}$ are the respective velocities of the truck frame at the start and end of the section considered.

Now, human impact is evaluated using the acceleration versus time signals treated according to the 2631-1 norm from the for Standardization (1997). For each human impact category and for the different calculation methods, the norm specifies the proper signals to use, filters and weightings to apply, and summation methods to rely on. In the end, the health hazard is measured by the Root Mean Square (RMS) of the treated signal. Table 1 reveals which signals are used for each measure presented here. The conservative measure only considers the vertical acceleration signal under the seat and uses Eq. (4) if

Table 1. Signals used to evaluate the different profile induced human impacts.

Criteria	Seat translation	Seat rotation	Backrest	Feet
Without backrest	x,y,z			
With backrest	x,y,z		x	
Conservative	z			
Comfort	x,y,z	x,y,z	x,y,z	x,y,z
Nausea	z			

that signal has a crest factor above 9. Also, where 4^{th} power is specified, the RMS value a_{w} is replaced by the following equation,

$$a_{\text{w}} = \left(\sum a_{\text{wi}}^4\right)^{1/4} \tag{4}$$

where a_{wi}^4 is the frequency weighted acceleration signal. The crest factor is defined by the norm as the ratio of the maximum instantaneous magnitude of the filtered signal over its RMS value.

At last, safety is evaluated by individually observing the evolution of the normal force under each tyre. The criteria considers the average distance travelled by each tyre with a tyre normal force below a given threshold. That threshold is a percentage of what the normal force would be if the truck were circulating on a perfectly smooth road. The 2 front wheels are considered separately from the others because they are crucial and less sensitive to the profile. They thus turn out to be a conservative result. The distance $d_{\text{saf},i}$ travelled by the truck with a wheel i with a force below the threshold is measured for each wheel according to the following equation,

$$d_{\text{saf},i} = \sum_j b_{i,j} \frac{x_{\text{cab},j+1} - x_{\text{cab},j-1}}{2} \tag{5}$$

where b_i, j is a boolean expression which is equal to one if and only if the normal force of wheel i at time j is below the threshold and $x_{\text{cab},j\pm1}$ is the cabin position at timestep $j \pm 1$. The criteria is the average value of $d_{\text{saf},i}$ taken over either the two front wheels or the twenty rear wheels.

2.2.2. Road profile rating

Various existing methods provide the means to rate roads by examining their longitudinal profiles. Some of these methods along with improved ones are presented, studied, and discussed.

First of all, the IRI is the most widely used method and is based on the Reference Quarter Car Simulation which uses the parameters of the *golden car* (Sayers and Karamihas 1998). The accumulated vertical movement of the *golden car*'s suspension when travelling at 80 km/h constitutes the IRI and has units of distance of vertical movement over distance travelled. The *golden car* is used for all the indices presented in this article. That said, the HRI is the IRI calculated using the average of the left and right track road profiles instead of being calculated using each track and then averaged. These two indices are presented in detail by Sayers and Karamihas (1998). Then, the FRI is identical to the HRI except that it takes the average profile elevation over 4 points instead

Table 2. Wavelength range breakdown of the various profile sets considered.

Profile set	Range (m)	Profile description	Qty
MTQ	[0.00, 91]	Real[a], provided by MTQ	54
Short (S)	[0.707, 2.83]	Bandpass filtered[b]	38
Medium (M)	[2.83, 11.3]	Bandpass filtered[b]	38
Long (L)	[11.3, 45.2]	Bandpass filtered[b]	38
IRI (I)	[0.25, 91]	Bandpass filtered[b]	38
Qualified (Q)	[0.00, 91]	Real[b], provided by MTQ	38
All (A)	Various	Real and filtered[c] profiles	233

[a]Two of the real profiles were constructed from the foward and backward repetition of a particularly irregular 91 m section taken from a profile.
[b]These categories only include profiles and their filtered derivatives which converged for every bandpass filtering presented.
[c]As opposed to the bandpass filtered profiles, this category includes every profile which converged without regard for their filtered derivatives.

of 2 and these points are chosen as the horizontal positions of the four wheels of a typical car. This index thus uses a typical passenger car wheelbase distance of 2.616 m. A truck wheelbase was avoided because the purpose is to have an index which can be used for all vehicles.

These three indices were calculated for the official MTQ profiles, which are only filtered by a high-pass filter at 91 m. Then, they are also calculated for the same MTQ profiles filtered in a way to isolate three different bandwidths. These bandwidths are: 1) the short wavelengths, from 0.707 m to 2.83 m; 2) the medium wavelengths, from 2.83 m to 11.3 m, 3) the long wavelengths, from 11.3 m to 45.2 m. In order to avoid a phase delay, two 3$^{\text{rd}}$ order Butterworth filters were applied sequentially on the forward and reversed signals. These bandwidths are established by researchers (Martel *et al.* 2011) who are able to predict the effect a specific road restoration procedure will have on each of the bandwidths. The various profile categories presented in this paper are made clear in Table 2.

Pushing the index development slightly further a Health Index based on the ISO-2631-1 guidelines was developed. It is defined as the RMS value of the weighted acceleration of the suspended mass of the *golden car*. It uses the conservative approach described earlier in Section 2.2.1.

A Wear Index is also developed. It yields a value D_{GC} which is equivalent to the damage accumulated by the suspension of the *golden car*. It is computed by the following equation,

$$D_{\text{GC}} = \sum_j ((2a_{\text{m},j})^3 n_{a_{\text{m},j}}) \tag{6}$$

where a_{m} is the acceleration of the quarter car's suspended mass, $a_{\text{m},j}$ is the magnitude of the acceleration a_{m} for which $n_{a_{\text{m},j}}$ cycles occur in the signal. Those 2 variables are obtained by a rainflow counting algorithm. These two indices are also measured on 2 and 4 points average profiles in the same fashion as for the HRI and FRI.

Finally, another index is implemented and is called the Safety Index. It is obtained by calculating the distance per kilometre of profile for which the spring representing the tyre

of the quarter car is stretched above a chosen threshold of 1.75 cm. It is only calculated on the original MTQ profile.

In order to clarify the 19 different indices which were just presented, Table 3 describes each of them individually. There, the term *simple* refers to indices which are presented as an average index between the left and right road tracks. The detailed calculation of each index is presented in Section A. The distribution of the profiles referred to as the Qualified profiles covers the range of IRI from very small at 0.68 m/km to quite large at 7.6 m/km. This is seen on Figure 3 which gives an insight on the range of indices tested and how they relate to each other by linking each index value to the value of the same profile for the other indices. The figure also shows that these profiles are evenly distributed in terms of Short Waves, Medium Waves, and Long Waves IRI. Conversely, the the Health, Wear, and Safety indices show some extreme values. Finally, the figure shows that strong Health and Wear indices are associated with a strong IRI and that the Health and Safety indices are closely related.

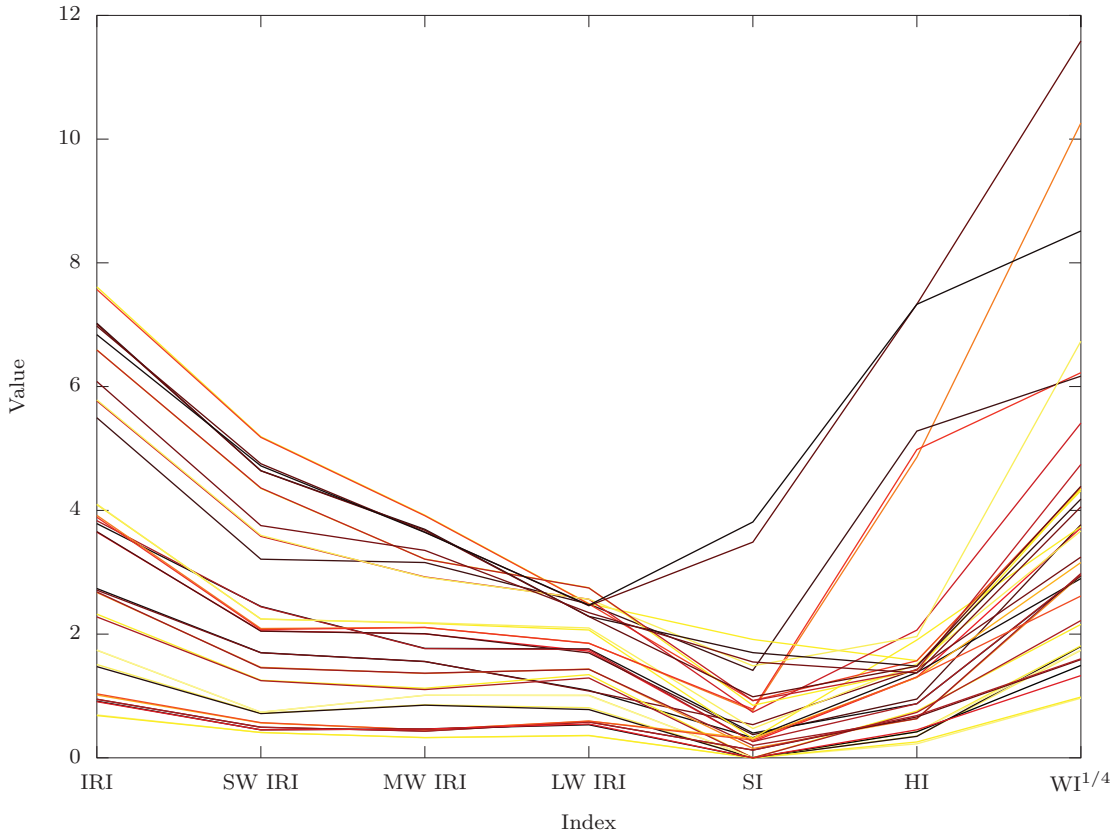

Figure 3. Distribution of the 38 Qualified profiles' IRI, short wave IRI (SWIRI), medium wave IRI (MWIRI), long wave IRI (LWIRI), Safety Index (SI), Health Index (HI), and the fourth root of the Wear Index ($WI^{1/4}$). The lines connecting the values have the purpose of linking the various indices of a same profile together.

Apart from being used to evaluate the indices, the filtered profiles are also used to run the full truck model. The purpose of doing so is to isolate the impacts that different bandwidths have on the vehicle. Furthermore, a supplementary bandpass filter is used

Table 3. The indices evaluated in this study.

Name	**Units**	**Description**
Simple Health Index[a]	m/s^2	weighted acceleration of the suspended mass of the *golden car*
IRI	m/km	International Roughness Index
Short Waves IRI	m/km	IRI of a filtered profile which retains the short wavelengths
Medium Waves IRI	m/km	IRI of a filtered profile which retains the medium wavelengths
Long Waves IRI	m/km	IRI of a filtered profile which retains the long wavelengths
Simple Wear Index[a]	$N^3 \cdot$ cycles	accumulated damage by the *golden car* suspension
Two point Health Index[a]	m/s^2	weighted acceleration of the suspended mass of the *golden car* circulating on the average profile of the left and right tyre tracks
HRI	m/km	IRI of the average profile of the left and right tyre tracks
Short Waves HRI[a]	m/km	HRI taken on a profile which was first averaged between left and right tyre tracks and then filtered to retain the short wavelengths
Medium Waves HRI[a]	m/km	HRI taken on a profile which was first averaged between left and right tyre tracks and then filtered to retain the medium wavelengths
Long Waves HRI[a]	m/km	HRI taken on a profile which was first averaged between left and right tyre tracks and then filtered to retain the long wavelengths
Two point Wear Index[a]	$N^3 \cdot$ cycles	accumulated damage by the *golden car* suspension circulating on the average profile of the left and right tyre tracks
Four point Health Index[a]	m/s^2	weighted acceleration of the suspended mass of the *golden car* circulating on the average profile of the left and right tyre tracks of the front and rear axles of a typical car
FRI[a]	m/km	IRI of the average profile of the left and right tyre tracks of the front and rear axles of a typical car
Short Waves FRI[a]	m/km	FRI taken on a profile which was first averaged between left and right tyre tracks of the front and rear axles of a typical car and then filtered to retain the short wavelengths
Medium Waves FRI[a]	m/km	FRI taken on a profile which was first averaged between left and right tyre tracks of the front and rear axles of a typical car and then filtered to retain the medium wavelengths
Long Waves FRI[a]	m/km	FRI taken on a profile which was first averaged between left and right tyre tracks of the front and rear axles of a typical car and then filtered to retain the long wavelengths
Four point Wear Index[a]	$N^3 \cdot$ cycles	accumulated damage by the *golden car* suspension circulating on the average profile of the left and right tyre tracks of the front and rear axles of a typical car
Simple Safety Index[a]	m/km	total distance for which the *golden car* tyre spring is stretched beyond a given threshold

[a]Index particular to this paper.

for the truck model. It is called the IRI filter and has a range of 250 mm to 91 m. It was chosen because such a filter is used in the standard IRI method. However, the developed truck model has a sensitive tyre model which has no need of the tyre filtering intended by the 250 mm low-pass filter.

3. Results and trends identified

This section summarises the trends that are obtained after testing every possible impact-index relation. To avoid redundancy, the bandpass filtered roughness indices are not taken on filtered profiles. When denoted as such, the curves have been normalised. The normalisation consists of plotting the results in terms of number of times of impact increase with respect to the lowest impact value recorded on the curve.

Most impact trends are presented by a correlation with a first degree polynomial having the form $f(x) = ax + b$ which are referred to as linear correlations. Some trends are however presented using a second degree polynomial having the form $f(x) = ax^2 + b$ and they are referred to as quadratic correlations. Higher order two-term polynomials were tested but did not yield better coefficients of determination.

Of the 270 profiles evaluated, the truck model converged for 233 of them. These 233 profiles are the ones referred to as All in Table 2. For consistency amongst different wavelengths, the 38 profiles shown as unfiltered or bandwidth filtered profiles are only the ones which converged for both the original and bandwidth filtered profile variants.

3.1. *Energy*

The best energy correlation came with the Simple Health Index and is shown on Figures 4 and 5. The quadratic correlation was of an equal coefficient of determination and the Simple Health Index gave the best correlation obtained amongst all indices for both linear and quadratic correlations. The two point Health Index gave the best cubic correlation with a $R \sim 0.89$. The Safety Index was also found to give a very good correlation ($R \sim 0.91$). It was found that long wavelengths have a very limited influence. Furthermore, the Medium Waves roughness indices correlated better with energy consumption by reaching a quadratic correlation of $R \sim 0.73$ with a tipping point at the value of 3 m/km. The results also highlight the fact that the regular IRI is unable to precisely predict energy consumption, as its coefficient of determination with fuel consumption was $R < 0.4$. Another fact worth noting is the presence of the two profiles generated by cycling in the forward and reverse directions of a subsection of a real profile. This particular profile severely excited the truck and produced an 80% energy consumption increase. It changed the correlation values for most of the indices in a way that made the Safety Index the best predictor by far when this profile was considered.

The results of Figure 4 agree well with what has been reported by Wambold (1985) who mentions that it is at excitation frequencies between 5 Hz and 20 Hz that most of the energy is dissipated in the vehicle. At 100 km/h those frequencies correspond to a bandwidth range of 1.7 m to 5.6 m which spans the short and medium wavelength range presented here. At last, Figure 5 shows how little impact the IRI filtering has on the calculated energy consumption. Thus, when Hammarström *et al.* (2012) mention that wavelengths between 5 mm and 0.5 m have a strong influence on vehicle energy consumption, wavelengths between 50 mm and 0.25 m can probably be excluded from that statement. This exclusion is justified because that range is the only difference between the Qualified and IRI profiles presented on Figure 5. Indeed, the IRI filter removes anything below 0.25 m and both profiles exclude anything below 50 mm due to the 25 mm sampling interval used by the MTQ.

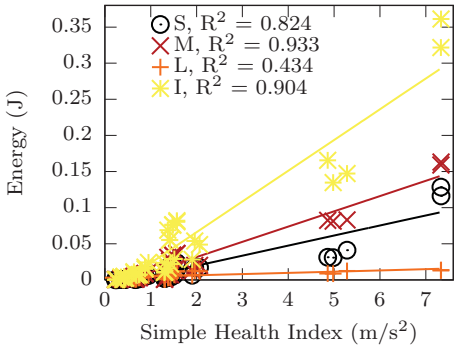

Figure 4. Linear correlations of normalised energy consumption against the Simple Health Index for short (S), medium (M), long (L) and IRI (I) wavelengths filtered profiles.

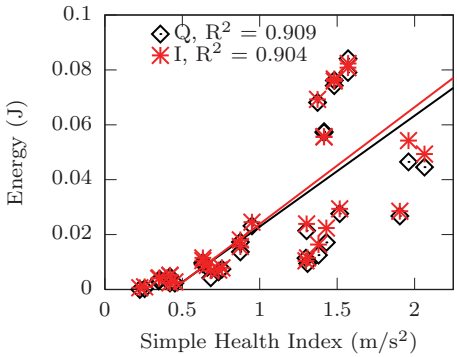

Figure 5. Lower portion of the linear correlations of normalised energy consumption against the Simple Health Index for Qualified (Q) and IRI (I) wavelengths filtered profiles.

3.2. *Health issues*

The best correlation between the impact of road roughness on the driver health and the Long Waves FRI is shown on Figure 6. As expected, the Long Waves IRI and Long Waves HRI also yield very good correlations with coefficients of determination $R^2 \sim 0.9$. The other indices and wavelengths, both linear and of higher order, give correlations with coefficients $R^2 < 0.5$. The best multi wavelength correlation comes from the FRI and it is shown on Figure 7. It clearly shows that long wavelengths have the most important impact on driver health while the medium and short wavelengths have low and negligible impacts, respectively.

In order to get more elaborate information on the health impact, selected relationships obtained by applying the ISO-2631-1 norm to the results of the Qualified profiles are presented. Of these, the Long Waves FRI is shown on Figure 8. Although coming short of expectations by presenting a more chaotic correlation, the Health Index is nevertheless shown on Figure 9. Both figures show that the conservative measure warns of a benign impact when compared to the less conservative methods. In fact, when the 3 vibrations in translation at the seat and the 3 at the backrest are considered, the measured impact on health more than doubles. Being even less conservative, the health impact measured

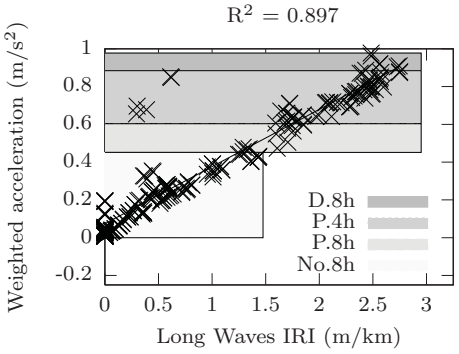

Figure 6. Linear correlation between the conservative impact on driver health and the Long Waves IRI with delimiters for zones of danger (D), possible danger (P), and no danger (No) after continued daily exposures of 4h and 8h.

on the signal processed by the 4$^{\text{nd}}$ degree power mean of Eq. (4) and using backrest vibrations will be roughly 4 times greater than the conservative measure. The results displayed here and the profiles of Figure 3 highlight the fact that the Health Index does not correlate with the IRI as the RMSA index presented by Sayers and Karamihas (1998) did. The possible explanation is that although both indices measure the RMS acceleration of the *golden car*, only the Health Index applies a frequency weighting to the seat signal.

Comfort showed good correlations with the IRI, HRI, and FRI whether they were filtered by bandpass filters or not. The relationship with Long Waves IRI is shown on Figure 10 where it is clear that the ride may be extremely uncomfortable and is at least very uncomfortable as soon as the Long Waves IRI reaches 2 m/km. If only the IRI is considered, the ride will be very uncomfortable at 4 m/km and extremely uncomfortable above 5 m/km. Comfort measured using the non-conservative power mean from Eq. (4) on the accelerations signals shows a more abrupt response by emphasising the measured impact of a brief perturbation. Whether occupants most dislike short and strong impact or repeated weaker impacts remains subjective. Also, Figures 8 to 10 show by the difference between driver and passenger that their seat adjustments and position in the vehicle have an observable impact on occupant health and comfort.

Figure 11 shows that the Long Waves IRI gives an approximation of the percentage of vehicle occupants that would suffer from a strong enough nausea to induce vomiting. Roughly one person out of twenty-five will be sick after circulating more than 6 h on a road with a Long Waves IRI greater than 2 m/km. The quality of the correlation with long wavelengths confirms that they are the most likely to cause nausea.

3.3. *Safety*

The Safety Index gives the best correlation for both All and Qualified profile sets. Both correlations appear on Figure 12 The Safety Index allows to join the data points that would otherwise seem to deviate from the mean. A 2$^{\text{nd}}$ degree curve would give a correlation of $R^2 = 0.93$ with All profiles. Conversely, the Four point Health Index which gives a very good safety correlation with the Qualified profiles at $R^2 = 0.89$ has a poor correlation with $R^2 = 0.20$ when All profiles are considered. This is due to the presence of two extreme profiles which seem to strongly excite a natural frequency of the vehicle.

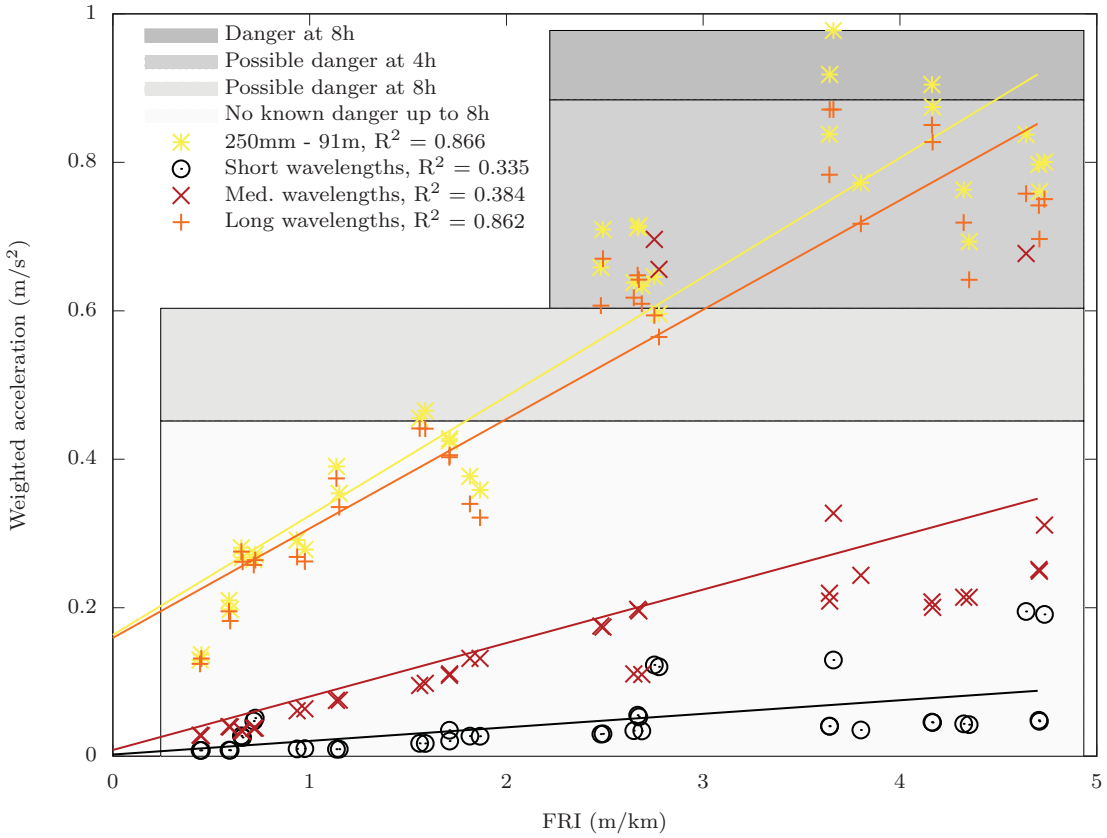

Figure 7. Linear correlations between conservative impact on driver health and the FRI with delimiters for zones of danger, possible danger, and no danger after continued daily exposures of 4h and 8h.

The medium wavelengths roughness indices all yield reasonable correlations for a 2nd degree curves, as shown for the Medium Waves HRI on Figure 13 where only the low range portion of the correlation is displayed. Finally, the relationship between IRI and safety is presented on Figure 14 where criteria values are truncated at a 3 m accumulated loss of contact distance. The figure allows to state that for IRI above 3 m/km, reductions of more than 70% of the friction force available at the front tyres almost certainly occur while for IRI below 3 m/km, such reductions almost certainly do not occur. It also shows that for IRI above 5.5 m/km there is most likely at least 2 m of accumulated distance of 70% reduced friction force. These IRI relationships agree very well with previous findings of Richard *et al.* (2009). The given distances on Figures 12 to 16 are the average distances per tyre for which the truck will travel on the 1 km long profile studied with a normal force equal or below 30% of the reference force.

Safety is also plotted against various criteria. On Figure 15 the relations between Medium Waves IRI and different levels of reduction of contact are shown. From that figure and the approach of Mayora and Piña (2009), it can be deduced that a profile alert should be generated when the Medium Waves IRI is above 1.5 m/km. Those authors generate an alert for Sideway-force Coefficient Routine Investigation Machine (SCRIM) values between 0.6 and 0.5, which means a normal force below 60% of its undisturbed

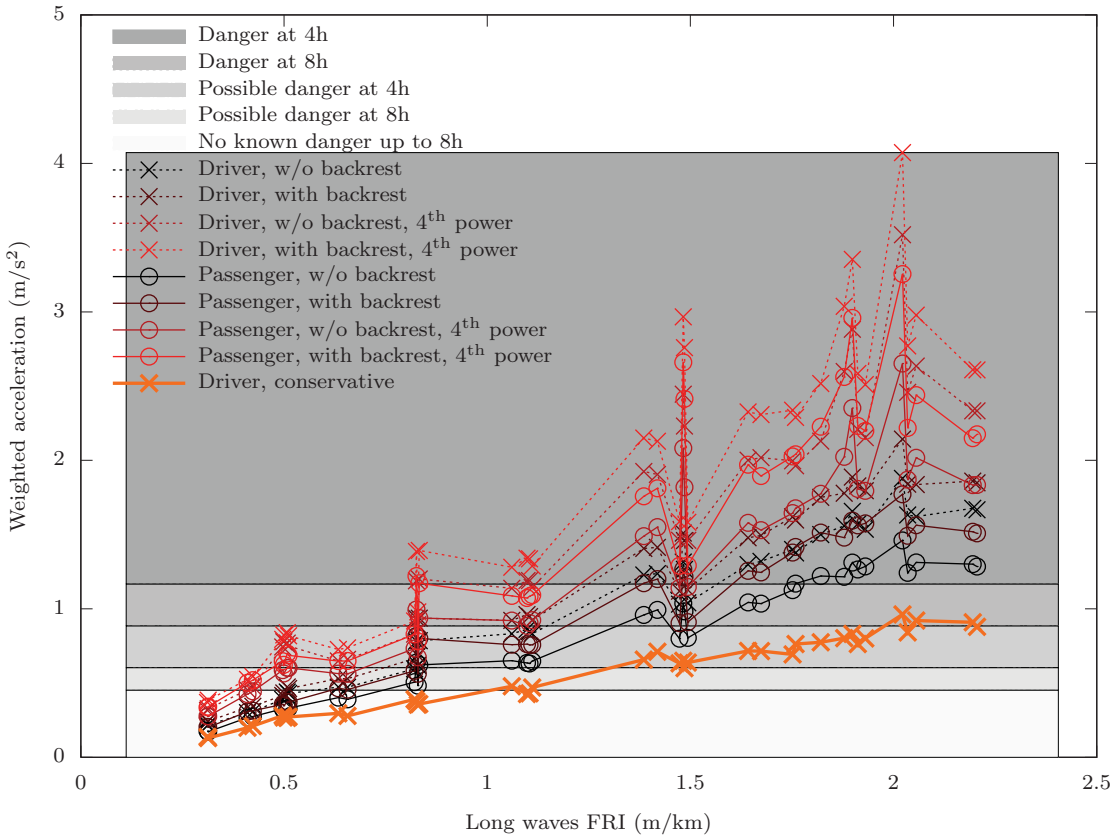

Figure 8. Relationship between the health impact on two different seats calculated according to various ISO-2631-1 methods and the Long Waves FRI.

value. Figure 15 also shows that the front wheels of the semitrailer truck will suffer from less substantial reductions of contact, which makes them a conservative result. Such a less substantial reduction was also shown by Fradette (2005). Finally, the figure shows that for a road having a Medium Waves IRI above 3.25 m/km, the wheels of each non-directing axle will retain only 60% of their contact force over at least 10% of their course. Referring again to Mayora and Piña's who consider that such a force reduction, however brief it may be, is important enough to generate an alert means that 10% of each profile with Medium Waves IRI above 3.25 m/km qualifies for an alert.

In the end, the best multi wavelength correlation was obtained with the Health Index and is presented on Figure 16, which shows that medium wavelengths have by far the most impact on safety while the long wavelengths do not have a significant influence on safety.

.

4. Conclusion

The relationships and conclusions brought up in this study apply for IRI and Index evaluations taken on 1 km road sections with impacts measured for a vehicle travelling at 100 km/h. The agreement with known findings from previous studies confirms the validity of the developed approach.

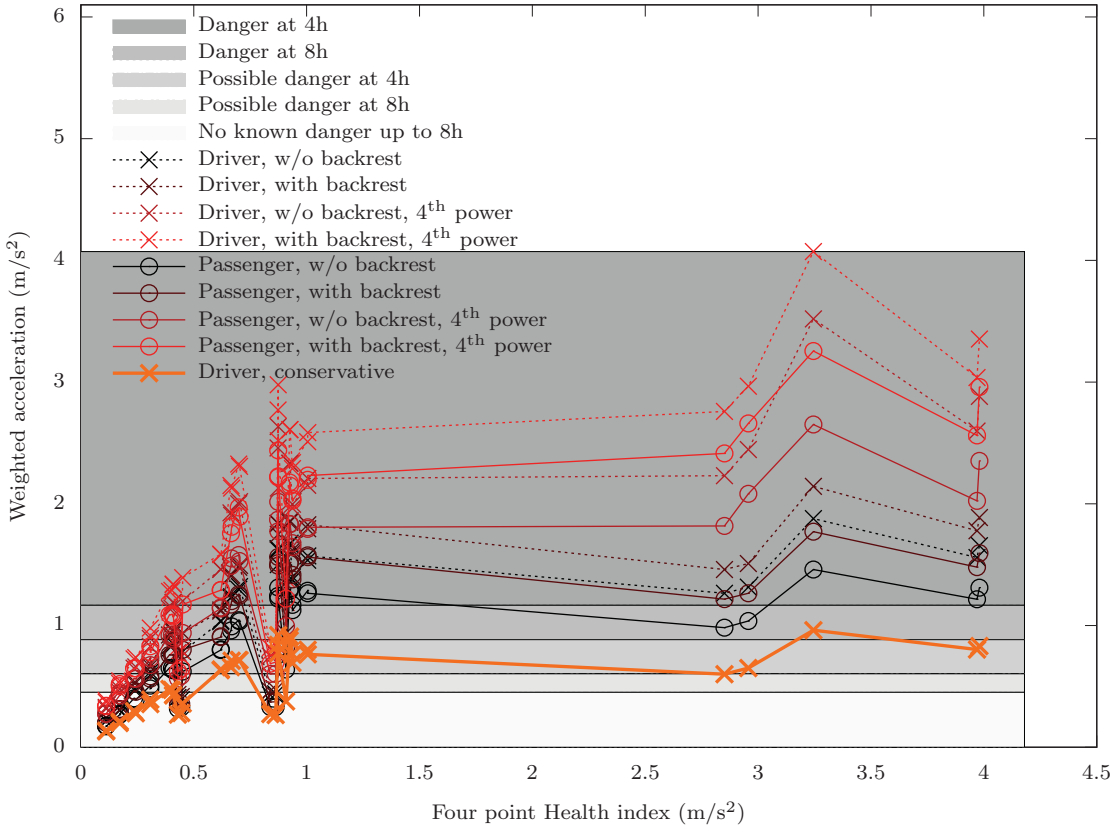

Figure 9. Relationship between the health impact on two different seats calculated according to various ISO-2631-1 methods and the Four point Health Index.

Even though energy consumption does increase with the IRI, it is not an adequate criteria for accurate fuel economy predictions. A reasonably accurate quadratic correlation indicates that above a Medium Waves IRI of 3 m/km the energy consumption critically increases. Yet, the Simple Health Index turns out to be the most efficient energy consumption predictor.

Long wavelengths are clearly the most influential on occupant wellbeing. Seat adjustments and positions do influence the effect on the occupant. The difference between the conservative measures and the more thorough assessments is quite large. It is almost certain that a vehicle occupant travelling on a road with a Long Waves FRI above 2 m/km at least 8 h per day over a period of many years will develop associated health problems. Seat adjustments may slightly mitigate that issue but as concluded by Granlund (2008) no vehicle suspension is able to isolate the driver from the road vibrations enough to significantly reduce health impacts. Also, chances that a vehicle occupant gets motion sickness caused by road deformations are small but do exist.

Safety correlates with medium wavelengths. In fact, above a Medium Waves IRI of 1 m/km, danger zones appear in the profiles. In a case where the IRI is the only available index, a value above 3 m/km indicates a problem while a value above 5.5 m/km is worth worrying about.

Both fuel efficiency and safety were sensible to extreme profiles which seemingly in-

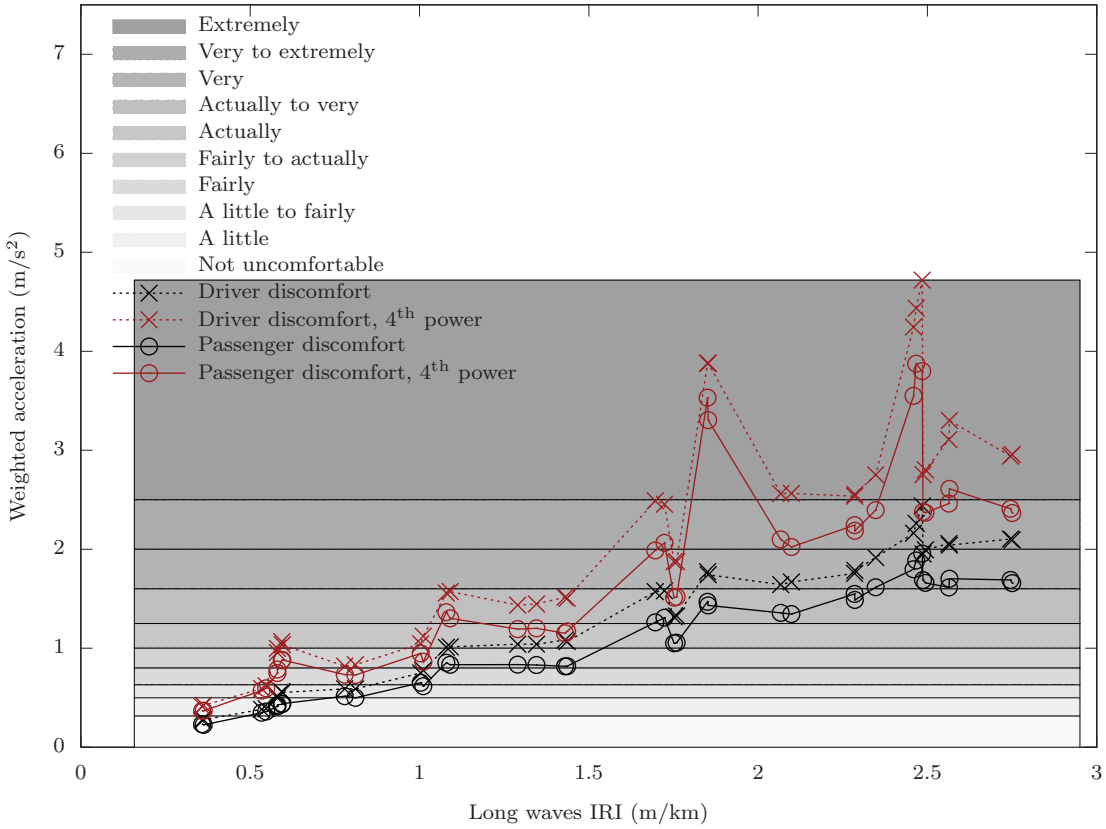

Figure 10. Relationship between the discomfort on two different seats calculated according to two ISO-2631-1 methods and the Long Waves IRI.

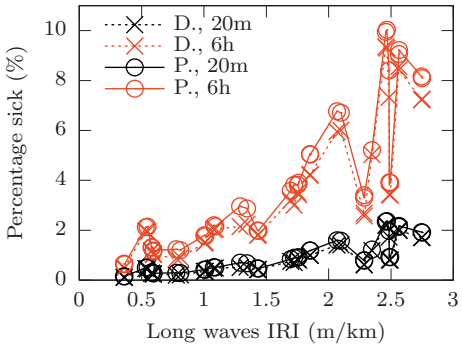

Figure 11. Relationship between the probability that untrained occupants will be sick from nausea and the Long Waves IRI for all profiles.

fluenced a vehicle's natural frequency in a way that the IRI was not able to predict. This weakness might in fact explain some of the IRI limitations. It is however expected that a real driver would adjust the velocity to avoid such resonance phenomena. Such

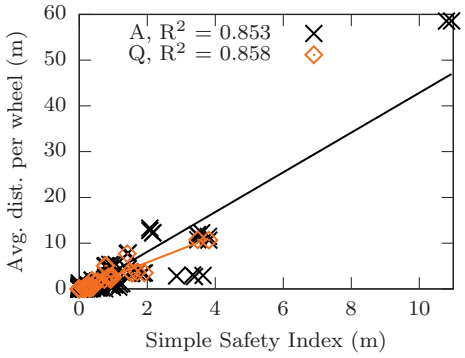

Figure 12. Safety impact : average distance travelled by each front wheel over the full profile with a normal force below 30% of the reference value for All (A) and Qualified (Q) profiles sets

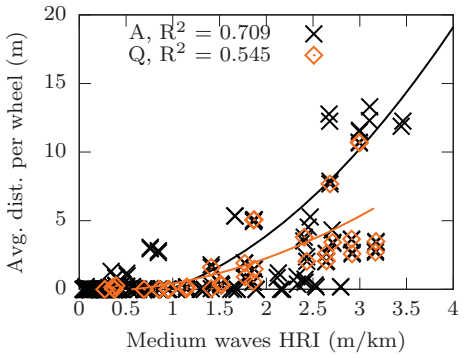

Figure 13. Lower portion of the correlation of the safety impact with the Medium Waves HRI for All (A) and Qualified (Q) profile sets.

phenomena are represented in this study by extreme outliers in the profile bank. They have an abnormally strong influence on the calculated impacts and tend to trigger an extreme response for at least one of the indices. Such deformations are usually quickly fixed by road managers and are thus not often seen on real roads. Nevertheless, they were included in this study because the capability to detect these profiles is what makes the tools presented here useful.

Further work should include a study of more wavelength decompositions, attempts at different index signal filtering, and a further look into the extreme profiles.

Acknowledgement(s)

The authors would like to recognise the financial support of the Natural Sciences and Engineering Research Council of Canada (NSERC) and the partners of the i3C industrial research chair. The valuable involvement of Michelin®, Politecnico di Milano, Freightliner®, Manac®, the Association du camionnage du Québec and the MTQ is also recognised.

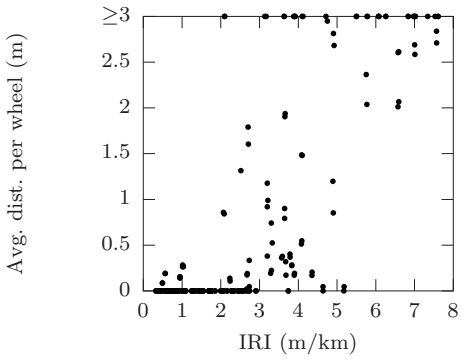

Figure 14. Safety impact : average distance travelled by each front wheel over the full profile with a normal force below 30% of the reference value.

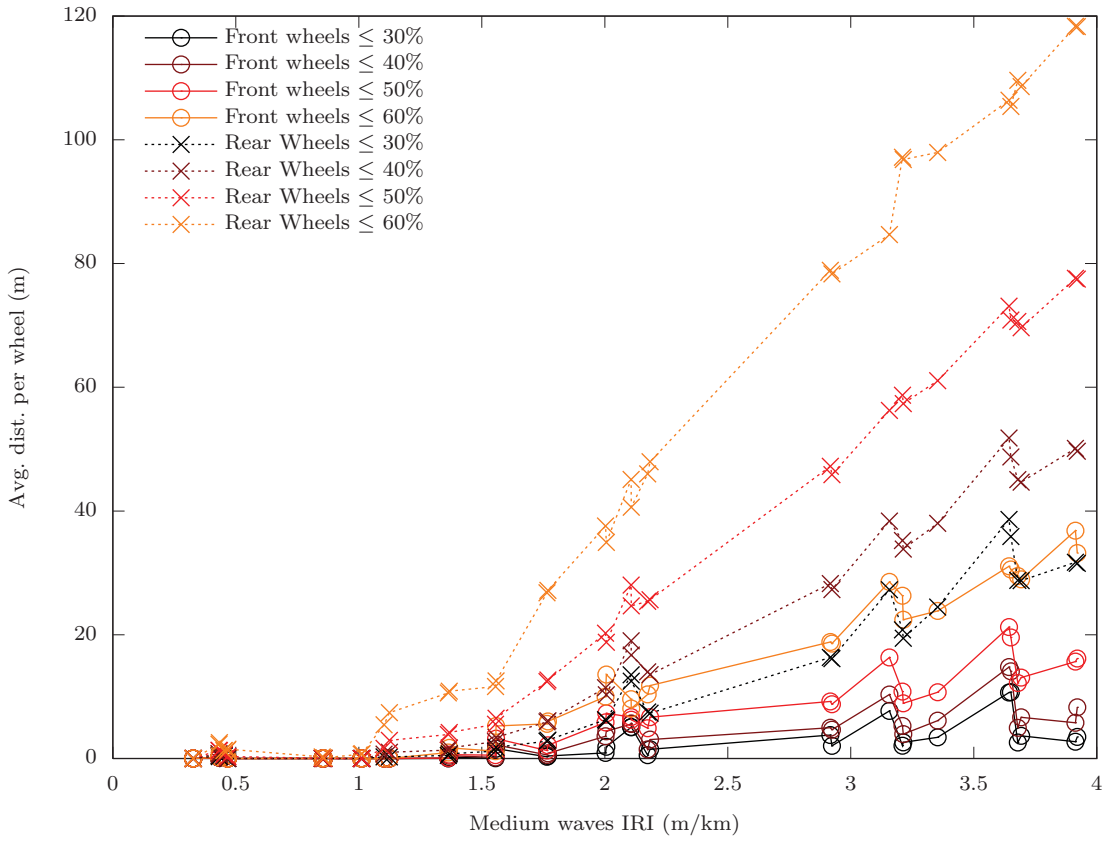

Figure 15. Relationships between various safety criteria and the Medium Waves IRI for the Qualified profile set.

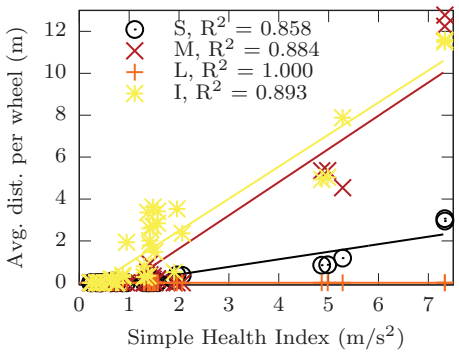

Figure 16. Linear correlations between safety and the Simple Health Index.

References

Allison, J.T., 2012. *Simulate and animate quarter-car suspension model* [online]. : . Available from: http://www.mathworks.com/matlabcentral/fileexchange/35478-simulation-and-animation-of-a-quarter-car-automotive-suspension-model [Accessed 2012].

Bester, C.J., 2003. The effect of road roughness on safety. *In*: *TRB 2003 Annual Meeting*.

Blundell, M. and Harty, D., 2004. *The multibody systems approach to vehicle dynamics*. Elsevier Limited.

Bouazara, M., L'influence des paramètres de suspension sur le comportement d'un véhicule. Master's thesis, Université Laval, 1991. .

Bouazara, M., 1997. Étude et analyse de la suspension active et semi-active des véhicules routiers. Thesis (PhD). Université Laval.

Delanne, Y., 1994. The influence of pavement evenness and macrotexture on fuel consumption. *Vehicle-road interaction*. American Society for Testing and Materials, 240–247.

Drollinger, R.A., 1987. Heavy duty truck aerodynamics. *SAE Technical Paper 870001*.

Fichera, G., Scionti, M., and Garesci, F., 2007. Experimental Correlation between the Road Roughness and the Comfort Perceived In Bus Cabins. *SAE Technical Paper*.

for Standardization, i.O., 1997. *Mechanical vibration and shock - Evaluation of human exposure to whole-body vibration - part 1: general requirements*. International Standard.

Fradette, N., Étude des conséquences de la détérioration des chaussées sur le comportement des véhicules et la sécurité des usagers de la route. Master's thesis, Université Laval, 2005. .

Fraggstedt, M., Power dissipation in car tyres. , 2006. , Technical report, Royal Institute of Technology, Stockholm.

Gagnon, D., *et al.*, L'incidence de l'uni et du type de chaussée sur le coût d'opération d'un véhicule, sur l'émission des gaz à effet de serre et sur la sécurité des usagers de la route. , 2006. , Technical report, Transport Canada.

Gagnon, L., *et al.*, 2012. An Implicit Rigid Ring Tire Model for Multibody Simulation with Energy Dissipation. *Submitted to Tire Science and Technology*.

Granlund, J., Health Issues Raised by Poorly Maintained Road Networks. , 2008. , Technical report, Swedish Road Administration Consulting Services.

Gualdi, S., Morandini, M., and Ghiringhelli, G.L., 2008. Anti-skid induced aircraft landing gear instability. *Aerospace Science and Technology*, 12 (8), 627–637.

Gyenes, L. and Mitchell, C.G.B., 1994. The effect of vehicle-road interaction on fuel consumption. *Vehicle-road interaction*. American Society for Testing and Materials, 225–239.

Hammarström, U., *et al.*, Coastdown measurement with 60-tonne truck and trailer: Estimation of transmission, rolling and air resistance. , 2012. , Technical report, VTI.

Imine, H., 2007. Heavy vehicle modeling, evaluation and prevention of rollover risk. *In*: *ECTRI, Young researcher seminar*, Brno, Czech Republic.

Jackson, N.M., Preliminary Report: An Evaluation of the Relationship between Fuel Consumption and Pavement Smoothness. , 2004. , Technical report, University of North Carolina.

Jackson, R.L., *et al.*, Synthesis of the effects of pavement properties on tire rolling resistance. , 2011. , Technical report, National Center for Asphalt Technology, Auburn University, Auburn, Alabama.

Kollman, J., Stability of a trailer during a lane change maneuver. , 2007. , Technical

report, Personal publication.

Lu, X.P., 1985. Effects of road roughness on vehicular rolling resistance. *Measuring road roughness and its effects on user and comfort: a symposium*. American Society for Testing and Materials, 143–161.

Martel, N., St-Laurent, S., and Parent, M., Projet de recherche sur l'utilisation des bandes d'ondes pour l'évaluation de l'uni au Québec. , 2011. , Technical report, Ministère des Transports du Québec.

Masarati, P., 2000. Comprehensive Multibody AeroServoElastic Analysis of Integrated Rotorcraft Active Controls. Thesis (PhD). Politecnico di Milano.

Masarati, P., 2012. *MBDyn 1.5 Source Code* [online]. : . Available from: www.mbdyn.org [Accessed 2012].

Masarati, P. and Morandini, M., 2010. Intrinsic deformable joints. *Multibody System Dynamics*, 23 (4), 361–386.

Masarati, P., Morandini, M., and Mantegazza, P., 2014. An efficient formulation for general-purpose multibody/multiphysics analysis. *in press of J. of Computational and Nonlinear Dynamics* Doi:10.1115/1.4025628.

Mayora, J.M.P. and Piña, R.J., 2009. An assessment of the skid resistance effect on traffic safety under wet-pavement conditions. *Accident Analysis and Prevention*, 41, 881–886.

McLean, J. and Foley, G., Road surface characteristics and condition: effects on road users. , 1998. , Technical report, ARRB Transport Research.

Miege, A.J.P. and Popov, A.A., 2005. The rolling resistance of truck tyres under a dynamic vertical load.. *Vehicle System Dynamics*, 43, 135–144.

Pacejka, H.B., 2006. *Tire and vehicle dynamics*. Society of Automotive Engineers.

Pehlivanidis, M. and St-Laurent, D., Plan de transport de l'Abitibi-Témiscamingue. , 2001. , Technical report, Ministère des Transports du Québec.

Rakheja, S., Ahmed, A.K.W., and Stiharu, I., Urban Bus Optimal Passive Suspension Study. , 2001. , Technical report, Concordia University.

Rhyne, T.B. and Cron, S.M., 2007. Tire energy loss from obstacle impact. *Tire Science and Technology*, 35 (2), 141–161.

Richard, M.J., *et al.*, 2009. Étude des conséquences de la détérioration de l'uni des chaussées sur le comportement des véhicules et la sécurité des usagers de la route. *Revue canadienne de génie civil*, 36 (3), 504–513.

Romão, F., *et al.*, 2003. Road traffic injuries in Mozambique. *Injury Control and Safety Promotion*, 10 (1-2), 63–67.

SAE, 2008. *Road load measurement using onboard anemometry and coastdown techniques*. Vol. J2263. Society of Automotive Engineers.

Sattaripour, A., 1977. The effect of road roughness on vehicle behaviour. *In*: *The dynamics of vehicles on roads and tracks*, Vienna, Austria.

Sayers, M.W. and Karamihas, S.M., 1998. *The little book of profiling*. UMTRI.

Schmeitz, A.J.C., 2004. A Semi-Empirical Three-Dimensional Model of the Pneumatic Tyre Rolling over Arbitrarily Uneven Road Surfaces. Thesis (PhD). Delft University of Technology.

Stenvall, H., Driving resistance analysis of long haulage trucks at Volvo. Master's thesis, Chalmers University of Technology, Göteborg, Sweden, 2010. .

Vassev, V., Étude des conséquences de la détérioration de l'uni des chaussées sur le comportement des véhicules. Master's thesis, Université Laval, 2005. .

Velinsky, S.A. and White, R.A., 1980. Vehicle energy dissipation due to road roughness. *Vehicle System Dynamics*, 9, 359–384.

Wambold, J.C., 1985. Road roughness effects on vehicle dynamics. *Measuring road rough-*

ness and its effects on user cost and comfort. American Society for Testing and Materials, 179–196.

WHO, World health report 2002: reducing risks, promoting healthy life. , 2002. , Technical report, World Health Organization, Geneva.

WHO, Health co-benefits of climate change mitigation - Transport sector. , 2011. , Technical report, World Health Organization.

WHO, Global status report on road safety 2013. , 2013. , Technical report, World Health Organization.

Appendix A. Methods for index calculation

The following scripts allow the calculation of the indices presented in the article.

This first script, written in the GNU Octave programming language and based on a quarter car simulation by Allison (2012), may be compatible with Matlab®. It allows the calculation of the regular IRI and the filtered IRI for the various bandwidths considered. It also gives the Health and Wear indices and the frequency content of the profile.

```
function [IRI FFT f] = getIRI(lane,dx,h)

% Initialize vehicle parameters for IRI (normalized data of the golden car)
k = 63.3;          % sprung mass spring stiffness
c = 6;             % sprung mass damper damping
kus = 653;         % tyre stiffness
v = 80/3.6;        % car velocity
mus = 0.15;        % unsprung mass
ms = 1;            % sprung mass
grav = 9.81;       % acceleration of gravity (m/s^2)
fcut = 4;          % cutoff frequency in oscillation per meter (ie: 4 = 0.25m
    lowest wavelength kept)
fcutP = 1/0.707;  % low wavelengths freq. for IRI bands
fcutM1 = 1/2.828; % freq. des longueurs d'ondes moyennes basses for IRI bands
fcutM2 = 1/11.312;% freq. des longueurs d'ondes moyennes hautes for IRI bands
fcutG = 1/45.248; % large wavelengths freq. for IRI bands
fcutGG = 1/91;     % simulation GMR/dynatest

% Construct linear state space model
Aqcar = [0 1 0 0;-kus/mus -c/mus k/mus c/mus;0 -1 0 1;0 c/ms -k/ms -c/ms];
Bqcar = [-1 0 0 0]'; Cqcar = [1 0 0 0; 0 1 0 0; 0 0 1 0; 0 0 0 1; 0 -1 0 1];
Dqcar = 0;
qcar = ss(Aqcar,Bqcar,Cqcar);

% note: y(:,1-4) = x, y(:,5) = d/dt susp stroke (i.e., x3dot)
% Definition of System States:
% x(1) = z1-z0 = L1      tyre deflection
% x(2) = z1dot           wheel cm velocity
% x(3) = z2-z1 = L2      suspension stroke (deflection)
% x(4) = z2dot           sprung mass velocity

% Initialize simulation
x0 = [0 0 0 0]';                          % initial state

% road profile data
dt = dx/v;                                    % simulation time step as in UMTRI
    Fortan script
road_z = h(:,lane)';
road_z -= h(1,lane);                          % start at 0 height
road_z = [zeros(1,ceil(ceil(11/dx))) road_z];% add 11m at start of profile as in
    UMTRI Fortran script

%filters,
pkg load signal; % for filtering
fnyq = 1/dx / 2; # Nyquist
```

```
road_z(2,:) = road_z(1,:);
[bfil,afil] = butter(3, [fcutM1/fnyq, fcutP/fnyq]);
road_z(3,:) = filtfilt(bfil, afil, road_z(1,:));
[bfil,afil] = butter(3, [fcutM2/fnyq, fcutM1/fnyq]);
road_z(4,:) = filtfilt(bfil, afil, road_z(1,:));
[bfil,afil] = butter(3, [fcutG/fnyq, fcutM2/fnyq]);
road_z(5,:) = filtfilt(bfil, afil, road_z(1,:));
[bfil,afil] = butter(3, fcut/fnyq); % tyre filter setup (250mm), applied inside next loop
%,filters

road_x = [0:dx:(size(road_z(1,:))(2)-1)*dx];     %using reference profile length as valid for all filtered profiles
tmax = road_x(end)/v;                            % simulation time length
dt2 = dx/v;                                      % time step for input data
t = 0:dt:tmax; x = v*t;                          % time/space steps to record output

for waveCnt = 2:1:5

        road_z(waveCnt,:) = filtfilt(bfil, afil, road_z(waveCnt,:));
        z0dot = [0 diff(road_z(waveCnt,:))/dt2];          % road profile velocity
        u = interp1(road_x,z0dot,x,'*linear','extrap');   % prepare simulation input
        % Simulate quarter car model,
        y = lsim(qcar,u,t,x0);
        deltamaxf = max(abs(y(:,1)));                     % max x3 amplitude
        z2dotdot = [0 diff(y(:,4))'/dt2];                 % sprung mass acceleration
        % get IRI,
        IRI(waveCnt) = sum(abs( diff(y(:,3)) ))/((x(end)-11)/1000);
endfor

if (1)  % enable to activate LRI (measures suspended mass accelerations as if it were a seat vibration for health indications)
        waveCnt = 1; % using unfiltered road for this type of evaluation
        z0dot = [0 diff(road_z(waveCnt,:))/dt2];          % road profile velocity
        u = interp1(road_x,z0dot,x,'*linear','extrap');   % prepare simulation input
        % Simulate quarter car model,
        y = lsim(qcar,u,t,x0);
        deltamaxf = max(abs(y(:,1)));                     % max x3 amplitude
        z2dotdot = [0 diff(y(:,4))'/dt2];                 % sprung mass acceleration
        % w_k freq weighting (ISO-2631-1),
        f1 = 0.4;   w1 = 2*pi*f1;
        f2 = 100;   w2 = 2*pi*f2;
        f3 = 12.5;  w3 = 2*pi*f3;
        f4 = 12.5;  w4 = 2*pi*f4;
        Q4 = 0.63;
        f5 = 2.37;  w5 = 2*pi*f5;
        Q5 = 0.91;
        f6 = 3.35;  w6 = 2*pi*f6;
        Q6 = 0.91;

        Hh_k = tf([1 0 0],[1 sqrt(2)*w1 w1^2]); % Hh (high pass)
        Hl_k = tf([0 0 w2^2],[1 sqrt(2)*w2 w2^2]); % Hl (low pass)
        Ht_k = tf([0 w4^2/w3 w4^2],[1 w4/Q4 w4^2]); % Ht (accel-vel transition)
        Hs_k = tf([1/w5^2 1/(Q5*w5) 1].*(w5/w6)^2,[1/w6^2 1/(Q6*w6) 1]); % Hs (upward step)

        Zseat = z2dotdot;       % this is not related to seat but rather to sprung mass
        Ts=dt;
        Hh = Hh_k; Hl = Hl_k; Ht = Ht_k; Hs = Hs_k;
        [num, den] = tfdata(Hl,'v');[B,A] = bilinear(num,den,Ts);Zseat_wk = filter(B, A, Zseat);[num, den] = tfdata(Hh,'v');[B,A] = bilinear(num,den,Ts);Zseat_wk = filter(B, A, Zseat_wk);[num, den] = tfdata(Ht,'v');[B,A] = bilinear(num,den,Ts);Zseat_wk = filter(B, A, Zseat_wk);[num, den] = tfdata(Hs,'v');
        a3_we = ( sum( Zseat_wk.^2 ) / length( Zseat_wk ) )^0.5; %RMS
```

```
100         a3_cr = max(abs(Zseat_wk)) / a3_we; %crest
101         a3_wf = ( sum( Zseat_wk.^4 ) / length( Zseat_wk ) )^0.25; % 4th power
102         if (a3_cr > 9)
103                 IRI(waveCnt) = a3_wf;
104         else
105                 IRI(waveCnt) = a3_we;
106         endif
107
108         if (2)
109                 waveCnt = 6; % rainflow counting on suspension force
110                 rf_suspension = rainflow(Zseat,t);
111                 Dmg_susp = sum((2.*rf_suspension(1,:)).^3.*rf_suspension(3,:));
112                 IRI(waveCnt) = Dmg_susp;
113         endif
114 endif
115
116 if (3)  % calculate fft of road
117         L = size(road_z)(2);
118         NFFT = 2^nextpow2(L);
119         Y = fft(road_z(1,:)-mean(road_z(1,:)),NFFT,2)/L;         % also setting
                mean to zero to avoid zero-freqency contribution of signal
120         f = 0;
121         FFT = 2*abs(Y(1:NFFT/2+1));
122 endif
123
124 endfunction
```

A similar script allows the calculation of the Safety Index. One difference is that the main function accepts an additional parameter, BMP, which is the elongation of the tyre spring beyond which the accumulation of the index value is effected. This elongation was set at 0.0175 m for the presented results. Thus, the differences from the previous script are that the function call is changed to,

```
1 function BM = getBoeingMod(lane,dx,h,BMP)
```

and the calculation of the index is done from the following lines of GNU Octave code,

```
1 if (4) % measure losses of contact with the road
2         BM = dx * size(find(y(:,1)' >= BMP))(2); % taking the total distance
              traveled with tyre-road spring streched above threshold (peak) WARNING
              : this is not an average, so will vary between profiles of different
              lengths!
3 endif
```

Finally, to obtain the simple, two, and four point indices, a GNU Octave procedure along the lines of what follows has been used to generate the average profiles prior to calculating the indices,

```
1  [IRI_L FFT_L f_L] = getIRI(1,delta,h(numPre:(size(h)(1)-numPost),:));
2  [IRI_R FFT_R f_R] = getIRI(2,delta,h(numPre:(size(h)(1)-numPost),:));
3  IRI = (IRI_L+IRI_R)/2;
4  FFT = (FFT_L+FFT_R)/2;
5  hMean = (h(:,1)+h(:,2))/2;
6  [HRI HFFT Hf] = getIRI(1,delta,hMean(numPre:(size(h)(1)-numPost),1));
7  WB = 2.616;      % ford focus 2002 wheelbase
8  numAdded = ceil(WB/delta/2)*2;  % added points to profile for front-rear mean
9  hMeanF = (( [hMean; hMean(end)*ones(numAdded,1)] + [hMean(1)*ones(numAdded,1);
       hMean] )/2)(numAdded/2:end-numAdded/2);
10 [FRI FFFT Ff] = getIRI(1,delta,hMeanF(numPre:(size(h)(1)-numPost),1));
```